Optical evidence of the layered array of grain boundaries in TGBA and TGBC mesophases

N. Isaert, L. Navailles, P. Barois, H. Nguyen

Classification
Physics Abstracts
61.30E — 61.70J — 62.20D

Optical evidence of the layered array of grain boundaries in TGB_A and TGB_C mesophases

N. Isaert ([1]), L. Navailles ([2]), P. Barois ([2]) and H. T. Nguyen ([2])

([1]) Laboratoire de Dynamique et Structure des Matériaux Moléculaires, Université des Sciences et Technologies de Lille, UFR de Physique, 59655 Villeneuve d'Ascq Cedex, France
([2]) Centre de Recherche Paul Pascal, CNRS, Avenue A. Schweitzer, 33600 Pessac, France

(*Received 15 March 1994, accepted in final form 9 June 1994*)

Résumé. — Nous présentons des mesures optiques de pas d'hélice dans des mésophases chirales cholestérique, smectiques torsadés par joints de grain (TGB_A et TGB_C) et smectique C hélicoïdal. Cette étude permet de discuter l'ordre des transitions de phases. De nouvelles lignes de défauts parallèles aux lignes de Grandjean-Cano sont observées dans les phases TGB uniquement. Elles sont interprétées comme des dislocations de l'empilement régulier des parois de joints de grain et donc comme une visualisation directe de leur existence. Leur origine et leur stabilité sont discutées grâce à un modèle élastique de déformation d'un TGB sous contrainte. Leur cœur est décrit comme une paroi formée de lignes de dislocations coin.

Abstract. — We report optical pitch measurements on chiral mesophases : cholesteric, twist grain boundary smectic (TGB_A and TGB_C) and helicoidal smectic C. The nature of the phase transitions is discussed. A new series of defect lines parallel to the usual Grandjean-Cano steps is observed in the TGB phases only. They are interpreted as edge dislocations of the layered array of smectic slabs stacked along the TGB screw axis and thus as a direct visual evidence of the Renn-Lubensky structure. Their origin and stability are discussed in an elastic model of strain of a TGB sample. Their core is described as a wall constituted of edge dislocation lines.

1. Introduction.

Following the predictions of de Gennes [1] and Renn and Lubensky [2-4] the discovery by Goodby and coworkers [5] of the helicoidal smectic A or Twist Grain Boundary Smectic A phase (TGB_A) in 1989 has opened a new way in research of liquid crystalline original phases. The TGB structure is now well characterized as the liquid crystal analog of the Abrikosov phase in type II superconductors. Slabs of smectic A material of thickness ℓ_b are regularly stacked in a helical fashion along an axis $\hat{P}$ parallel to the smectic layers. Adjacent slabs are continuously connected *via* a grain boundary constituted of a grid of parallel equispaced screw dislocation lines analogous to magnetic vortices. The finite twist angle of each grain boundary

is $\Delta\theta = 2 \tan^{-1} (d/2 \ell_d) \approx d/\ell_d$, where d is the smectic period and ℓ_d the separation of parallel screw dislocation lines.

In 1991 Goodby's group obtained this phase in different series with several kinds of polymorphism [6, 7]. The Bordeaux group has synthesized several tolan series in which the TGB_A phase appears in various sequences such as Crystal (K)-helicoidal Smectic C (S_{C*})-TGB_A-Isotropic (I) [8] or K-S_{C*}-smectic A (SA)-TGB_A-Cholesteric (N*)-Blue phases (BP)-I [9]. In the series presented in reference [9], the S_{C*} phase is absent for short lateral chains whereas BP and N* disappear for long ones.

In the following series ($nF_2BTFO_1M_7$) [10] :

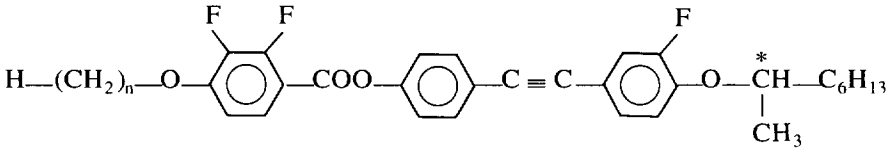

we have observed and characterized a new TGB phase predicted by Renn and Lubensky [3, 4] namely the twist grain boundary smectic C phase (TGB_C) in which the TGB slabs are constituted of tilted smectic C material.

The first proof of the discontinuously twisted structure proposed by Renn and Lubensky [2] — lattice of screw dislocations connecting a twisted stack of smectic slabs — has been given by Ihn *et al.* [11] by electron microscopy on freeze fracture experiments. Navailles *et al.* [12] have performed X-ray experiments at thermal equilibrium on well aligned TGB_C samples of 12 $F_2BTFO_1M_7$ and observed a commensurate lockin of the size of the smectic slab on the helical pitch.

Several complementary studies (DSC, phase diagram of binary mixtures, electro-optical studies, X-ray diffraction) reported in our previous publications [10, 12] have clearly identified the TGB phases of the $nF_2BTFO_1M_7$ series. In the present paper, we focus our attention on the variations of the helicity in the S_{C*}, N*, TGB_A and TGB_C phases of the 10, 11 and 12 $F_2BTFO_1M_7$ and point out some relationship between the nature of the transitions and the helicity. In section 3, we report optical observations of new defects which bring direct visual evidence of the existence of a regular stack of slabs along the screw axis. These observations are discussed and analysed within the frame of a simple elastic model proposed in section 4. The nature of the new defects is discussed in section 5.

2. Behaviour of the helical twist at the phase transitions.

Helical pitch measurements were performed in thin wedges made of two flat 1 mm thick pieces of glass. The glass plates were thoroughly cleaned with absolute ethanol and dried. The planar alignment was promoted by a simple gentle unidirectional buffing of the glass substrate with a velvet fabric. No polymer coating was used. Thin wedges were formed with two 20 × 20 mm plates assembled with a 0.15 mm spacer at one end. The resulting wedge angles were then calibrated by optical reflection of monochromatic light. Typical values were about 0.5-0.6 degrees. The cells were then filled by capillarity in the isotropic phase and introduced in a FP5 Mettler hot stage fitted on a Leitz Ortholux polarizing microscope in the transmission mode. The samples were cooled down to the cholesteric phase where regular arrays of Grandjean steps formed rapidly. The residual temperature gradient was estimated from the motion of the phase boundaries and was less than 0.05 °C per millimeter during the pitch measurements. In order to improve the accuracy of previous experiments reported in reference [10], particular attention was paid to the stability of the temperature and to the quality of the

thermal equilibrium during the measurements : cooling rates were never higher than 0.2 °C/mn in or near the TGB phase.

Finally, in the S_{C^*} phase, the helical pitch was measured from similar observation of Grandjean-Cano steps with a homeotropic geometry. In calibrated wedged cells made of clean buffed glass plates, homeotropic alignment was often spontaneously achieved in samples cooled down to the S_{C^*} phase and improved by gentle back and forth motion of the upper plate. Were also used homeotropic drops deposited on a rubbed glass plate, which often exhibited linear Grandjean-Cano defects and/or fringes of equal thickness with a period equal to the pitch or half-pitch (for further details, see Ref. [13]). Displacements of these defects or fringes have been particularly useful to precise rapid variations of the S_{C^*} pitch close to the TGB_A phase.

• For $n = 10$, the phase sequence is K-S_{C^*}-TGB_A-N*-BP-I on heating. Most of the data about the helical pitch have been given previously in reference [10]. The pitch is continuous at the N*-TGB_A transition in spite of a rather energetic transition. It increases on cooling in the TGBA phase and diverges on approaching the S_{C^*} phase. This divergence is related to the second order nature of the transition. Here we specify the variation of the pitch in the S_{C^*} phase. It exhibits a steep decrease close to TGB_A which is usually characteristic of a second order S_{C^*} S_A transition (Fig. 1a).

• For $n = 11$, the sequence is K-S_{C^*}-TGB_C-TGB_A-N*-BP-I on heating. Several complementary observations support a second order TGB_A-TGB_C transition : i) the enthalpy signal is very weak [10], ii) the pitch of the S_{C^*} phase increases on approaching the S_{C^*}-TGB_C transition (Fig. 1b). Nevertheless iii) when the sample is heated so rapidly that the TGB_C phase does not have the time to develop over the whole sample, it is possible to observe unstable S_{C^*} regions in which the pitch falls off abruptly. This is again the signature of a nearby second order S_C-S_A transition (Fig. 1b). Lastly iv) there is no discontinuity of the smectic layer spacing neither at the TGB_A-TGB_C nor at the TGB_C-S_{C^*} transition [10].

We present in figure 1b new careful measurements of the helical pitch $P(T)$ which also support a second order TGB_C-TGB_A transition for the compound $n = 11$. No anomaly of the pitch is detected at the N*-TGB_A transition. The TGB_A-TGB_C transition is marked by a steep but continuous variation of the pitch. We misinterpreted this sharp evolution as a discontinuity in reference [10]. A very slow heating or cooling rate reveals in fact that it is possible to keep the same system of Grandjean-Cano (GC) lines while passing through the transition. The GC lattice continuously expands itself without any destruction from TGB_A to TGB_C. The first photograph (Fig. 2) shows this continuous transformation in a weak temperature gradient (less than 0.05 °C/mm perpendicular to the GC lines). The variation is however very abrupt and the graph $P(T)$ is presumably characterized by a quasi vertical tangent at the transition point.

Finally, we note that the pitch diverges in the TGB_C phase when approaching the almost second order TGB_C-S_{C^*} transition.

• The last compound $n = 12$ exhibits the sequence K-S_{C^*}-TGB_C-N*-BP-I. Like for $n = 11$, the pitch in the S_{C^*} phase increases in a monotonic way on heating (Fig. 1c). On the TGB_C side, the pitch diverges again on approaching the S_{C^*} phase. The inset in figure 1d shows that the inverse pitch $1/P$ varies almost linearly with temperature throughout the TGB_C phase.

A noticeable discontinuity is observed at the N*-TGB_C transition : the second photograph (Fig. 3) clearly shows two kinds of GC steps in a weak temperature gradient. A decrease of the temperature destroys one sort of steps before it generates the other, unlike what is observed with the $n = 11$ compound at the TGB_A-TGB_C transition.

The values of the pitch given in figure 1c were recorded by the Grandjean-Cano method and are much more accurate than those previously deduced from the rotatory power [10] (we had actually not been able to prepare regular GC steps in our first experiments). Knowing the

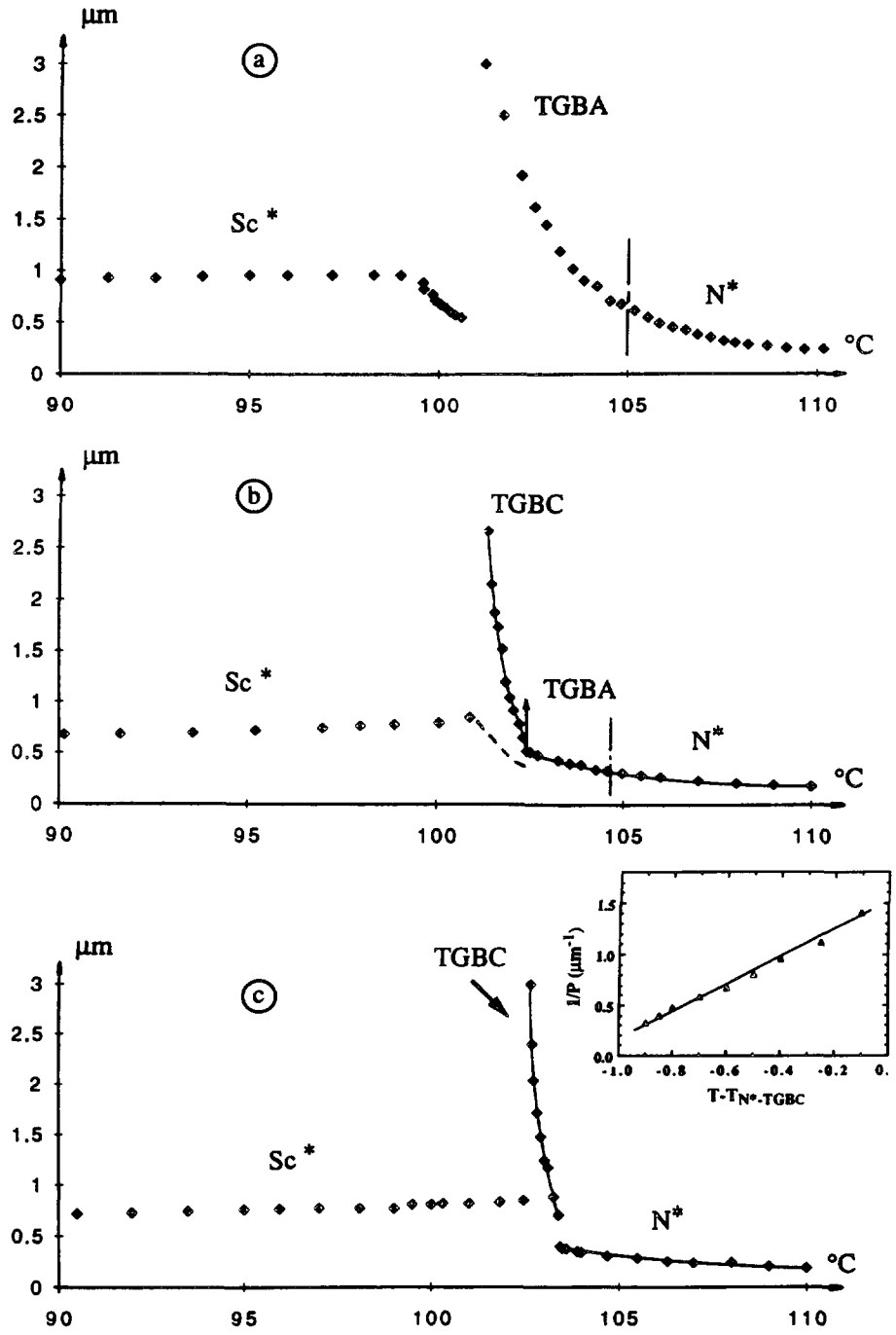

Fig. 1. — Helical pitch variation *versus* temperature for homologous compounds of the series $nF_2BTFO_1M_7$ (a) $n = 10$, (b) $n = 11$. The decrease steep of the pitch in the S_{C^*} phase (dashed line extending over the TGB domain) is observed at high heating rate only. (c) $n = 12$. At low temperature the pitch of the S_{C^*} phase increases up to 1.22 µm at 60 °C for $n = 10$, 0.87 µm at 50 °C for $n = 11$ and 1.00 µm at 40 °C for $n = 12$ (not represented in the figure). Inset points out the linear variation of the inverse pitch $1/P$ in the TGB_C phase of $n = 12$ (*versus* $T - T_{N^* TGB_C}$) with a slope of 1.25 turn.μ^{-1} °C^{-1}

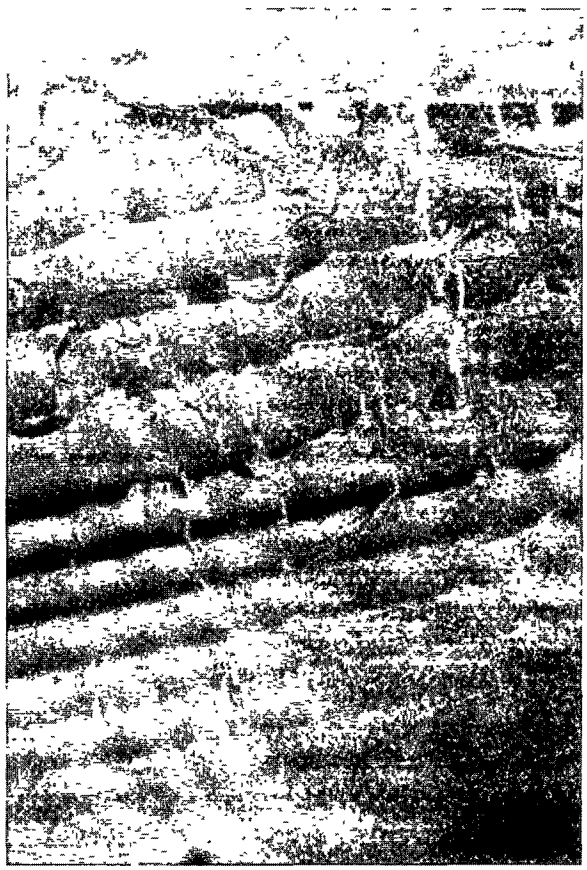

Fig. 2. — Photograph of the TGB_A-TGB_C transition in the Cano wedge with planar boundary conditions. The size of the photograph is 220 × 330 μm, $n = 11$, $T = 102.6$ °C with a gradient of about 0.05 °C from top to bottom. Narrow Grandjean-Cano steps in the TGB_A phase (bottom) continuously transform into wider steps in the TGB_C phase (top). The helical pitch is continuous at this transition.

values of the grain boundary angle $\Delta\theta$ for the TGB_C phase of the $n = 12$ compound [12], we can infer the size ℓ_b of the smectic slabs along the screw axis : it grows from 47 nm at the N*-TGB_C transition ($\Delta\theta = 2\pi/16$, $P = 0.75$ μm) to 150 nm at the S_{C^*} frontier ($\Delta\theta = 2\pi/20$, $P = 3.0$ μm). The corresponding distances between screw dislocations in the grain boundaries are 9.4 nm and 11.8 nm, respectively [12]. The values of the ℓ_b/ℓ_d ratio ($5.0 \leqslant \ell_b/\ell_d \leqslant 12.7$) are thus significantly larger than 1 expected from the RL model [2].

3. Observation of dislocations in the regular array of grain boundaries : slab-dislocations.

The prismatic samples used for pitch measurements contain, parallel to the edge of the prism, generally perfectly visible Grandjean-Cano lines (Figs. 2, 3). In the TGB phases, it is possible to visualize other lines, almost regularly distributed, parallel to the GC steps but with a shorter spacing. Their contrast is generally much improved when the polarizer is set at 45° from the buffing direction and a $\lambda/4$ plate is inserted just before the analyzer set parallel to the polarizer (Fig. 4, to be compared with Fig. 3). Anticipating the model developed in the next section, we

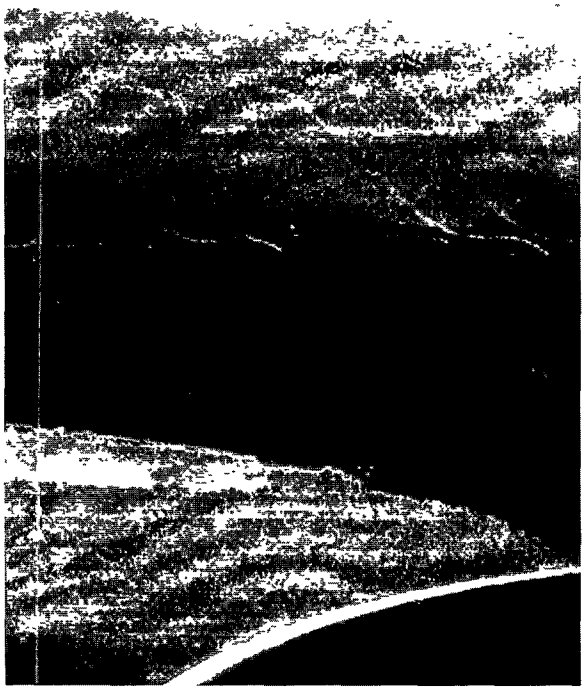

Fig. 3. — $n = 12$, $T = 103.3$ °C, photograph size 220×330 μm. Cholesteric-TGB_C transition for 12 $F_2BTFO_1M_7$ in a weak temperature gradient (about 0.05 °C from top to bottom). The regular array of narrow Grandjean-Cano steps in the cholesteric phase breaks apart at the transition. A new array of wider steps appears in the TGB_C phase. The pitch is discontinuous at this transition.

interpret these new lines as edge dislocations of the layered array of smectic slabs : each little line is associated with a jump of the number of slabs in the finite thickness of the prismatic sample (Figs. 8, 9). Just as the GC lines show the layered symmetry of the cholesteric structure, these new dislocations constitute a direct visual evidence of an additional layering along the screw axis.

This visual proof adds up to X-ray studies performed on the TGB_C phase of the last compound $n = 12$ [12]. The observed commensurate lockin of this TGB phase allowed a direct X-ray measurement of the finite rotation angle of the slabs $\Delta\theta$. In the case of all reported TGB_A phases and of the TGB_C phase of the shorter compound $n = 11$, X-ray studies indicate that the structure is incommensurate [12, 13] and the present optical observations constitute the only evidence of the existence of a stack of smectic slabs along the screw axis. We have indeed observed these slab-dislocations in the TGB_C phases of both commensurate $n = 12$ (Fig. 4) and incommensurate $n = 11$ (Fig. 5). On the other hand, for the TGB_A phase of $n = 10$, the slab dislocations only appear on the first GC steps in the thinner region of the wedge (Fig. 6). This feature will be explained by the model developed in the next section.

Fig. 4. — $n = 12$, $T = 103.1$ °C, photograph size 220 × 330 μm, $\lambda/4$ plate inserted. The sample is the same as in figure 3. A new series of parallel lines (little arrows) appears between the Grandjean-Cano steps (big arrows) of the TGB_C phase of 12 $F_2BTFO_1M_7$. These new defects are interpreted as edge dislocations of the layered array of smectic slabs (or equivalently grain boundaries) forming the TGB structure. We call them slab-dislocations.

In the TGB_C phase of the $n = 12$ compound, we finally remark that the number of slab-dislocations per pitch (~ 10-12) is lower than the number of slabs in a pitch counted on X-ray diffraction patterns (16, 18 or 20 [12]). This will also be explained in the next section.

4. Elastic behaviour of a TGB material in a wedge.

The texture of a cholesteric sample in a wedge with planar boundary conditions has been studied extensively [14-16]. The cholesteric structure can be viewed as a layered material with layers of thickness $P/2$ perpendicular to the screw axis (heli-layers). In such a picture, weak elastic distortions can be described by a coarse grained elastic model [17] like in a smectic sample. The elastic moduli of compression B and bending K of the cholesteric layers are simply related to the Frank constants of twist K_2 and bend K_3 by $B = K_2(2\pi/P)^2$ and $K = 3/8\, K_3$ [17]. The Grandjean-Cano lines are nothing but edge dislocation lines of this layered structure.

Fig. 5. — $n = 11$, $T = 102.2$ °C, photograph size 220 × 330 μm, $\lambda/4$ plate inserted. Grandjean-Cano lines (big arrows) and slab-dislocations (little arrows) in the TGB_C phase of 11 $F_2BTFO_1M_7$.

In smectics, regular arrays of edge dislocations in wedges have been observed and studied in detail by several authors [18-20]. The strain field due to the presence of an isolated dislocation in an infinite medium was first calculated by de Gennes [21]. Pershan [22] and Nallet and Prost [19] argued that the strain field is basically the same in the confined geometry of a wedge of weak angle. The curvature strain is almost negligible outside a parabola $x_\parallel^2 = 4\,\lambda\,|x_\perp|$ ($x_\parallel$ is a coordinate parallel to the layers and perpendicular to the dislocation core, $x_\perp$ is a coordinate perpendicular to the layers and $\lambda = \sqrt{K/B}$ is the smectic penetration length).

Following Nallet and Prost [19], the energy of each dislocation can be written as the sum of three terms : a wedge confinement energy E_W which originates from the strain field outside the parabola, a far field energy E_F representing the energy inside the parabola and a core energy E_C. The far field and core contribution $E_F + E_C$ is proportional to the linear extension of the GC line and will be referred to as a line energy. It depends on the Burgers vectors b of the dislocation whereas the wedge contribution E_W also depends on its position.

We now want to describe the array of GC lines in a TGB material. Like in a cholesteric or a smectic, we need to estimate the elastic energy of strain but three parameters are now required. We choose the pitch P, the size ℓ_b of the smectic slabs along the screw axis and the smectic period d. Other parameters such as the rotation angle $\Delta\theta$ between two adjacent slabs or the

Fig. 6. — $n = 10$, $T = 100.5$ °C, photograph size 220 × 330 μm, $\lambda/4$ plate inserted. The Grandjean-Cano steps of the TGB_A phase of 10 $F_2BTFO_1M_7$ (big arrows) embrase several scarcely visible slab-dislocations (little arrows).

distance ℓ_d between screw dislocations within a grain boundary follow :

$$\Delta\theta = 2\,\pi\ell_b/P$$

$$\ell_d = d/(2\tan(\Delta\theta/2)). \qquad (1)$$

Let us emphasize at this stage that with our approach we have identified three different layerings in the TGB material : i) the heli-layers of thickness P (a few hundreds of nm) correspond to helical periods of the director and are perpendicular to the screw axis $\hat{P}$ like in a cholesteric ii) the slab-layers form a regular stack of period ℓ_b (a few tens of nm) along $\hat{P}$ and are characteristic of the TGB structure iii) finally the conventional smectic layers of thickness d (a few nm) are found in each block.

We denote by P_0, ℓ_{b0} and d_0 the unstrained values of the pitch, of the size of the smectic slabs and of the smectic period, respectively. We first remark that the smectic period d is controlled by a molecular length and thus expected to experience very small deviations from d_0. We will therefore restrict our attention to the other two strains i.e. $P - P_0$ and $\ell_b - \ell_{b0}$. P_0 and ℓ_{b0} depend on temperature only for a given TGB sample. The energy density

of weak isotherm elastic compressions of the TGB structure is then $\Delta f_{TGB} = f_{TGB}(P, \ell_b) - f_{TGB}(P_0, \ell_{b0})$. We finally assume for the moment that we are dealing with an incommensurate TGB phase for which the free energy density f_{TGB} is expected to be analytic and can be derived twice with respect to P and ℓ_b. This property is certainly false in the case of a commensurate TGB since the lockin terms in the free energy density are non-analytic. This yields a phenomenological form of the elastic energy density of compression :

$$\begin{aligned}\Delta f_{TGB} &= f_{TGB}(P, \ell_b) - f_{TGB}(P_0, \ell_{b0}) \\ &= \frac{B_1}{2}\left(\frac{P - P_0}{P_0}\right)^2 + \frac{B_2}{2}\left(\frac{\ell_b - \ell_{b0}}{\ell_{b0}}\right)^2 - B_{12}\left(\frac{P - P_0}{P_0}\right)\left(\frac{\ell_b - \ell_{b0}}{\ell_{b0}}\right).\end{aligned} \tag{2}$$

The elastic coefficients B_1, B_2 and B_{12} are the second derivatives of f_{TGB} at the minimum (P_0, ℓ_{b0}). The first part of the integral describes compressions of the pitch just like in a cholesteric. The elastic constant B_1 is thus expected to be of order $K_2(2\pi/P_0)^2$. The second term describes variations of the size of the smectic slabs at constant pitch. Physically, it depends only on the interaction energy of the screw dislocations since their density $\sim (\ell_b \ell_d)^{-1}$ is a function of P only. Lastly, the coupling term B_{12} is allowed by symmetry and has to be added.

Cartesian coordinates (x, y, z) are well-appropriate to our experimental geometry. We choose x along the bisector and y parallel to the edge of the wedge (Fig. 7). Planar boundary conditions insure that the screw axis is essentially along z. The free energy density (2) can be diagonalized and integrated over the volume of the sample. It reads (per unit length along y) :

$$\Delta F_{TGB} = \int dx\, h(x) \frac{1}{2}\left\{\frac{(B_1 B_2 - B_{12}^2)}{B_2}\left(\frac{P - P_0}{P_0}\right)^2 + B_2\left(\left(\frac{\ell_0 - \ell_{b0}}{\ell_{b0}}\right) - C\left(\frac{P - P_0}{P_0}\right)\right)^2\right\} \tag{3}$$

with $B_2 > 0$, $B_1 B_2 - B_{12}^2 > 0$ and $C = B_{12}/B_2$. $h(x) = \alpha x$ is the thickness of the sample in a wedge of weak angle α.

We are left with two uncoupled variables with respect to which ΔF_{TGB} can be minimized separately. Minimization with respect to $(P - P_0)$ is analogous to the problem of a cholesteric in a wedge. It generates a network of edge dislocation lines as follows. Let $N(x)$ be the number of helical periods $P(x)/2$ along z at abscissa x (and thickness $h(x)$) :

$$N(x)\frac{P(x)}{2} = h(x) = \alpha x . \tag{4}$$

Following Nallet and Prost [19], we can divide the sample into basic cells containing only one dislocation line (Fig. 7) : cell number j contains the j^{th} dislocation of Burgers vector b_j at position X_j. The number of $P/2$ units jumps from $N_j = 1 + \sum_{i=1}^{j-1} b_i$ to $N_{j+1} = N_j + b_j$. It extends from abscissa x_j defined by $h(x_j) = N_j P_0/2$ to x_{j+1} for which $h(x_{j+1}) = N_{j+1} P_0/2$ (i.e. the elastic stress is zero at x_j and x_{j+1}).

Minimization of $\Delta F_{TGB}[P - P_0]$ with respect to the position X_j of the j^{th} dislocation line is straightforward. It yields :

$$\frac{2\alpha X_j}{P_0} = N_j + \frac{b_j N_j}{2N_j + b_j} . \tag{5}$$

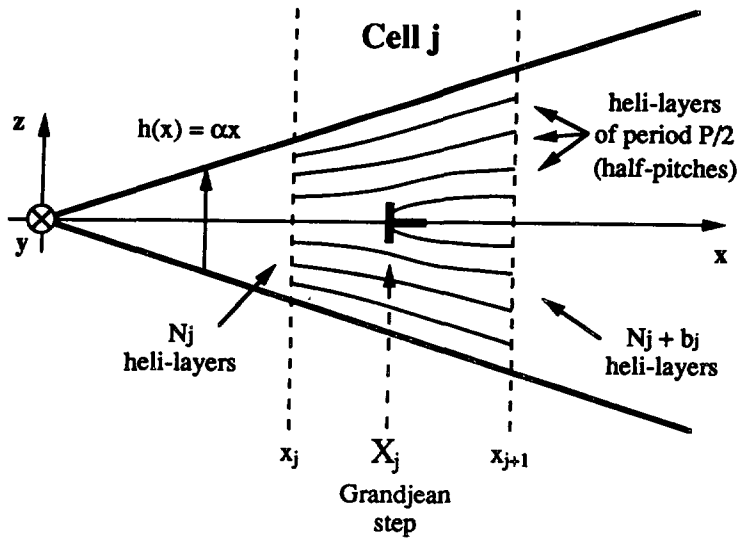

Fig. 7. — Schematic representation of the cholesteric layers in a Cano wedge of weak angle α. The sample is divided into basic cells containing one Grandjean step i.e. one edge dislocation of the heli-layers of period $P/2$. Cell number j is represented here. The sample thickness $h(x)\alpha x =$ is exactly N_j and $N_j + b_j$ times the unstrained value of the period $P_0/2$ at the boundaries of the cell x_j and x_{j+1} respectively. The position X_j of the Grandjean step is obtained by minimization of the elastic energy of compression (see text, Eq. (6)).

Minimization with respect to the Burgers vectors b_j remains in principle to be performed to describe the array of dislocations completely. The line energies $E_F + E_C$ have to be included which requires the knowledge of their dependence on b_j. Like in a cholesteric, the value of b_j is expected to change in the sample if the line energies increase slower than $b(E_C \sim \text{Ln } b$ for instance in a lyotropic smectic [19] whereas Friedel and Kléman showed that E_C depends on the way the dislocation is dissociated at short scale into two disclination lines [23]).

A calculation of the b dependence of the line energies in a TGB phase is beyond the scope of this paper and will not be needed. We shall only assume that the regular array of dislocations exists in the well aligned TGB material and consider a particular (and constant) value of b for simplicity. Optical pitch measurements reported in section 1 are consistent with Grandjean-Cano lines of Burgers vector 1. We shall therefore retain this value in the following (note that N_j simply equals j in this case). Our conclusions can easily be extended to $b = 2$.

Before minimizing ΔF_{TGB} (Eq. (3)) with respect to the second independent variable $V = \left(\frac{\ell_b - \ell_{b0}}{\ell_{b0}} \right) - C \left(\frac{P - P_0}{P_0} \right)$, it is worth noting that the physically acceptable values of the ratio $C = B_{12}/B_2$ are between 0 and 1 : equations (1) show that elastic variations of the pitch P arise from combined variations of $\Delta\theta$ and ℓ_b. The two extreme situations are variations of P at constant ℓ_b (P and ℓ_b are decoupled in this case and $C = 0$) and variations of P at constant twist angle $\Delta\theta$ (relative variation of P and ℓ_b are strictly equal and $C = 1$).

We can now proceed with the minimization of (3) with respect to V. Let us consider a volume of TGB material between two adjacent GC lines of rank $j - 1$ and j. The system is conveniently described by the reduced abscissa $r = 2\,\alpha x/P_0$ (Fig. 8). With the assumption

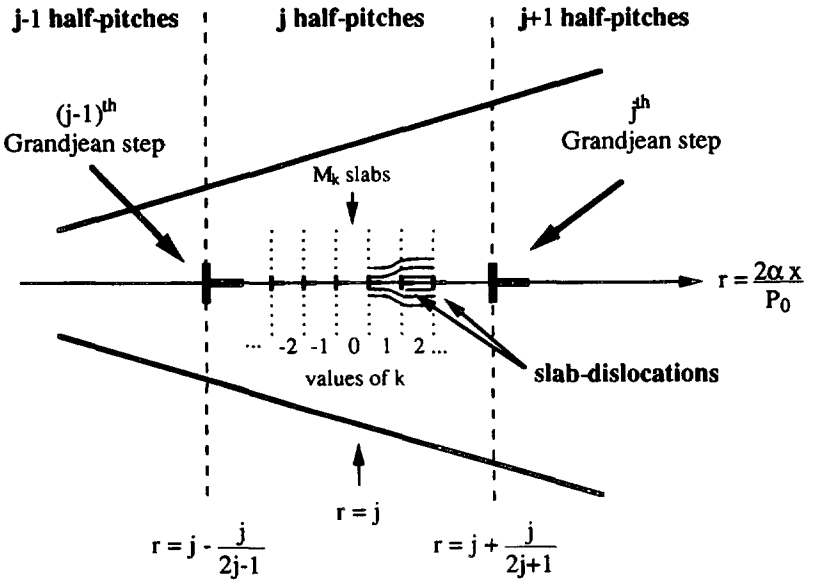

Fig. 8. — TGB material in the Cano wedge of weak angle α in between two adjacent Grandjean-Cano steps of rank $j-1$ and j. The reduced abscissa is defined as $r = \alpha x/P_0$ in which P_0 is the unstrained value of the helical pitch. The number of periods (heli-layers or half-pitches) is j whereas the number of smectic slabs is M_k ($k = k_{min}, \quad -1, 0, 1, \quad k_{max}$) of order $j/2\ P_0/\ell_{b0}$. A slab-dislocation defect is represented between $k = 1$ and $k = 2$.

$b_j = 1$, this cell extends from reduced abscissa $j - j/(2j-1)$ to $j + j(2j+1)$. The number of $P/2$ units (i.e. half pitches) is j and the helical pitch is unstrained at abscissa $r = j$ only.

We now remark that the finite thickness $h(x)$ of the wedge at abscissa x (or r) contains an integer number of slabs M_k. In an unstrained TGB, M_k is expected to be close to the natural irrational value $\tilde{M}_0$ defined as :

$$\tilde{M}_0 = j\,\frac{P_0}{2\,\ell_{b0}} = \frac{j}{2}\,q_0 \tag{6}$$

in which q_0 is the natural number of smectic slabs in a pitch of unstrained TGB [2]. We define M_0 as the closest integer to $\tilde{M}_0$ and choose $M_k = M_0 + k$:

$$h(x) = \alpha x = (M_0 + k)\,\ell_b(x) = j\,\frac{P(x)}{2} \tag{7}$$

Variations of the number of slabs $M_0 + k$ within the cell of rank j can occur through integer steps of value β_k (i.e. all values of k may not be physically present). The associated defect lines can again be viewed as edge dislocations of Burgers vector β_k of the layered structure of TGB smectic slabs (Fig. 8). They will be referred to as slab-dislocations. Furthermore, equation (6) shows that the average variation of the number of slabs from cell j to $j+1$ is $q_0/2$ (the elastic stress would diverge with j otherwise). The GC lines are thus also slab-dislocation lines of order $q_0/2 - \sum_k^{\text{cell } j} \beta_k$.

The variable V and the elastic free energy of compression (3) can be calculated for all possible values of k. The variable V reads :

$$V(r, k) = \frac{r}{j}\left(\frac{\tilde{M}_0}{M_0 + k} - C\right) - 1 + C \tag{8}$$

with

$$C = \frac{B_{12}}{B_2} \quad 0 \leqslant C \leqslant 1$$

V is zero for a set of values $\{r_k\}$ of the reduced abscissa. The free energy is shown in figure 9. It is a set of parabolae centered at positions r_k :

$$\frac{B_2}{2} V^2(r, k) = \frac{B_2}{2}\frac{1}{j^2}\left(\frac{\tilde{M}_0}{M_0 + k} - C\right)^2 (r - r_k)^2 \tag{9}$$

with

$$r_k = j + \frac{j(M_0 - \tilde{M}_0 + k)}{\tilde{M}_0 - C(M_0 + k)} \tag{10}$$

The extreme values of k in cell j correspond to $r_{k_{\min}}$ and $r_{k_{\max}}$ as close as possible to $j - j/(2j - 1)$ and $j + j/(2j + 1)$ respectively.

If the line energies are omitted, the ground state is given by the lowest branches of the parabolae (Fig. 9). The slab-dislocation lines are located at the intersection of two adjacent parabolae of rank k and $k + 1$. The Burgers vectors β_k all equal 1. The number $N_{sd}(j)$ of such lines in the cell j is :

$$N_{sd}(j) = k_{\max} - k_{\min} \approx \text{Int}\left[(1 - C)\left(\frac{q_0}{2} + \frac{\tilde{M}_0 - M_0}{j}\right)\frac{1}{1 - \left(\frac{1 + C}{2j}\right)^2}\right]$$

$$\approx (1 - C)\frac{q_0}{2}. \tag{11}$$

In which Int $[x]$ stands for integer part of x. In all cases, $N_{sd}(j)$ is of order $(1 - C)\, q_0/2$. The number of lines of zero tension thus gives an estimate of the coupling constant C is q_0 can be determined independently.

In the case of the $n = 12$ compound, both numbers are available : $q_0 = 16$, 18 or 20 [2] whereas the observed number of slab-dislocations is 5 or 6. C is then of order 0.25 to 0.75 if negligible lines tensions are assumed which, as we shall see later, is legitimate in this case.

If the line energies $\gamma(\beta_k)$ (i.e. energy of the slab dislocation defect per unit length along direction y) are included, the system may prefer form fewer lines (i.e. β_k is then larger than one) : two lines of Burgers vector $\beta_k = \beta_{k+1} = 1$ are replaced by one double $\beta_k = 2$ if the excess elastic cost of compression is less than the gain in line energy (the branch of parabola of rank $k + 1$ becomes unphysical). The number of slab-dislocation lines is then divided by two Increasing further the line energy will reduce the number of lines until eventually they disappear completely (note that the situation is actually slightly more complex since the slab-dislocations removed from cell j have to be included in the GC steps).

In a wedge geometry, the elastic stress falls off with increasing thickness (Eq. (9)). As a result, the slab-dislocations must become unstable beyond some critical thickness for which

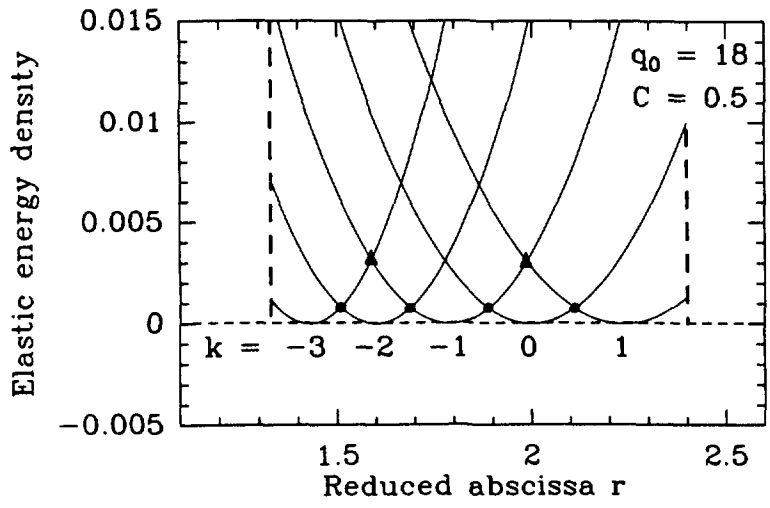

Fig. 9. — Elastic energy density (in $B_2 P_0^2$ units) along the wedge (reduced abscissa $r = \alpha x/P_0$ is used) represented for $j = 2$ (two half pitches) $q_0 = 18$ and $C = 0.5$. The Grandjean-Cano steps of rank 1 and 2 limit this cell at position $r = 2 - 2/3$ and $2 + 2/5$ (heavy dashed lines). For each possible value of k (5 values here) the elastic energy density is a parabola centered at position r_k. If the line energy is omitted, the lowest branches constitute the ground state with 4 slab-dislocations located at the intersection of the parabolae (heavy dots). When the line energies are included, other states of higher elastic energy but with fewer defects may be stable : the three branches $k = -3$, -1 and 1 for instance would form a state with 2 slab-dislocations only (triangles). For very high line energies (above j_{limit}, see text) no slab-dislocation forms and a single parabola is physical. The corresponding energy equals the line energy at $j = j_{limit}$.

the energy γ of the last line (of Burgers vector of order $(1 - C)\, q_0/4$) matches the excess elastic energy of compression in a cell. Estimating these two-energies yields the critical thickness j_{limit} (in $P_0/2$ units) :

$$j_{limit} = \frac{(1 - C)^2}{96\,\alpha} \frac{B_2 P_0^2}{\gamma} \tag{12}$$

This limit depends on the angle α of the wedge (of order 10^{-2} in our experiments). It was actually observed in the TGB_A phase of the $n = 10$ compound : as mentioned in section 3, the slab-dislocation lines do not show up for cell thicknesses above 2 to 3 pitches which yields $j_{limit} \approx 5 \approx (1 - C)^2 B_2 P_0^2/\gamma$. Below the limit (i.e. j lower than but close to j_{limit}) slab-dislocations are observed and their number N_{sd} is controlled by the balance between two unknown quantities $B_2 P_0^2$ and γ. N_{sd} cannot be related to C and q_0 by equation (11).

On the other hand, the ratio $(1 - C)^2 B_2 P_0^2/\gamma$ is significantly higher for TGB_C samples ($n = 11$ and $n = 12$) since slab-dislocation lines were observed for all thicknesses up to 9-10 pitches (i.e. j_{limit} is larger than 20) with the same angle α. This situation corresponds to the other limit (of negligible line tension) for which equation (11) holds. Comparing the number of lines $N_{sd}(5, 6)$ to $q_0/2$ (8 to 10) yields an estimate of the coupling ratio $C = B_{12}/B_2$. $0.25 < C < 0.75$ whereas $B_2 P_0^2/\gamma$ is larger than 80 for TGB_C samples.

A more accurate description of the stability of the slab-dislocation defects requires a realistic calculation of the line energies γ *versus* Burgers number β_k (note that the value of β_k is not even mentioned in the rough estimate of Eq. (12)). We shall see in the next section that the structure of the defects is actually more complex than the usual strain field of compression and bending associated with a simple edge dislocation in a layered material. We will not calculate the line energy but propose a qualitative structure of the defect.

In principle, the present model does not apply to commensurate TGB materials for which the elastic energy density cannot be differentiated. A non-analytic contribution defined on rational values of the ratio P/ℓ_b superimposes to the elastic free energy density Δf_{TGB} of equation (3). The ground state is locked on the lowest energy ratio P_0/ℓ_{b0} from which « excited » states differ by finite amounts of the variables P and ℓ_b. A correct description of the distortion of a commensurate structure is clearly very complex. The qualitative behaviour may however be similar to that described above if the finite differences between all possible states of comparable energy are small enough to reproduce quasi continuous variations. Furthermore in the commensurate case, the variables P and ℓ_b may vary by steps of different lockin values along the z coordinate i.e. across the thickness of the sample allowing finely varying average values along x. The experimental behaviour of the $n = 12$ compound, reported commensurate elsewhere [12] is indeed quite similar to the incommensurate $n = 10$ and $n = 11$ compounds. We deduce from this observation that the conclusions of the present discussion qualitatively apply to the commensurate TGB_C phase of the compound $n = 12$.

5. Core structure of the slab-dislocations.

Figure 10 shows a slab-dislocation defect across which the number of slabs changes from M_k to M_{k+1} (a unit Burgers vector is considered for simplicity). If strong planar anchoring conditions are assumed, the total twist of the director across the thickness of the sample is constant equal to $j\pi$ (j half-pitches). It follows that the average grain boundary angle $\Delta\theta$ changes from $2\pi j/(M_k - 1)$ to $\Delta\theta' = 2\pi j/M_k$. The density of screw dislocation lines in the grain boundaries is thus lowered by a factor $(M_k - 1)/M_k$ whereas the number of grain boundaries is increased by the inverse factor $M_k/(M_{k-1})$. As a result, the total number of dislocation lines remains constant across the defect. A proportion $1/M_k$ of the screw dislocations leave each of the M_{k-1} existing grain boundaries to merge into a new one. To do so, they must travel parallel to the smectic layers and become hence edge dislocations (see inset of Fig. 10). It follows that the core of the defect is a wall rather than a line.

Furthermore, a continuous connexion of the slab-layers across the defect implies a small rotation of the smectic layers ($i(\Delta\theta' - \Delta\theta)$ for slab number i, see Fig. 10). The array of edge dislocation forming the defect wall produces the required rotations [23] as shown (inset of Fig. 10). Note that the density of edge dislocations in the wall increases on approaching the inserted slab.

It must be emphasized that the conservation of the dislocation lines is of course not specific to the defect wall we just described. It is a general rule that dislocations cannot end in the bulk of a smectic material (or more generally in any ordered structure). The screw dislocations must either go through the defect wall or turn backwards and form a hairpin loop. We just argued that the first situation is met in the slab-dislocation wall, the second one corresponds to the GC defects.

In the present picture, the slab-dislocation wall extends over the whole thickness h of the sample from one glass plate to the other. One may imagine a more localized core of limited extension $L_z < h$ along z. In such a case, the grain boundary angle would not remain constant across the sample thickness ($\Delta\theta'$ for the slabs facing the defect wall but still $\Delta\theta$ for the others).

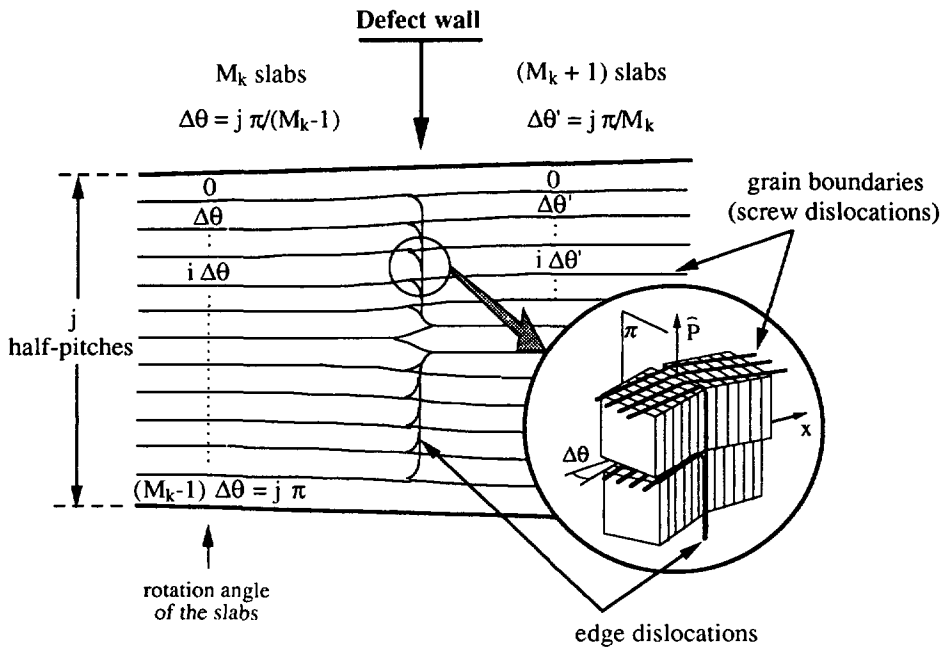

Fig. 10. — Proposed structure of a slab-dislocation defect in a wedge with planar boundary conditions. The pitch axis $\vec{P}$ is vertical and perpendicular to the walls of the wedge (thick lines). The thin horizontal lines are perpendicular to the pitch direction and represent the layered array of grain boundaries (screw dislocations). The number of smectic slabs jumps from M_k to $M_k + 1$ (a unit Burgers vector is considered for simplicity) whereas the rotation of the director across the thickness of the sample remains constant ($j\,\pi$ for j half-pitches). The grain boundary angle $\Delta\theta$ between adjacent TGB slabs jumps from $\pi j/(M_k - 1)$ to $\pi j/M_k$. A proportion $1/M_k$ of the screw dislocations leave the $M_k - 1$ existing grain boundaries (vertical lines) to merge into a new one. The inset shows that they must travel parallel to the smectic layers to leave a grain boundary : they become hence edge dislocations in the interspace between grain boundaries. Furthermore, these edge components generate the required rotation of the smectic layers (see insert). The core of the defect is a wall of such edge dislocation lines (plane π of inset).

The actual value of L_- depends on the balance between the gain in core energy and the cost in elastic energy.

Finally, we discuss briefly the case of weak anchoring conditions at the surface. The strain of the helical structure generates a torque which tends to rotate the director on the surface by an angle $\delta\theta$ away from the buffing direction. It follows that the total twist across the sample $j\,\pi + \delta\theta$ is no longer constant. The difference in grain boundary angle $\Delta\theta' - \Delta\theta$ is hence lowered which in turn implies a lower density of edge dislocations in the defect wall and a lower core energy γ. The experiments reported in the present paper may well correspond to this case of weak planar anchoring conditions since the alignment was promoted without polymer coating (residual oily defects which are visible in Figs. 5 and 6 do not show up when a buffed PVA coating is used). Furthermore, a constant total twist ($j\,\pi$) across the wedged sample implies a linear variation of the pitch with thickness and thus a regular evolution of the reflected color within adjacent GC lines. We observed instead that the reflected colors changed by steps across the slab-dislocations. This suggests that the total twist experiences a little discontinuity at the slab-dislocation defect.

6. Conclusion.

In the present paper, we have reported new careful optical measurements of the helical pitch in well-aligned TGB_A and TGB_C mesophases of the series $nF_2BTFO_1M_7$ in a Cano wedge. The pitch variations are continuous with temperature at the cholesteric-TGB_A and TGB_A-TGB_C transitions ($n = 10$ and $n = 11$ compounds) but discontinuous when a direct cholesteric-TGB_C transition occurs ($n = 12$).

In the TGB mesophases, optical observations in the thin part of wedges of weak angle show regular array of new defects appearing between the Grandjean-Cano lines, parallel to them.

In the case of an incommensurate TGB phase, the overall structure of the strained sample was shown to be conveniently described by a simple elastic model of compression of two coupled layered systems, namely the cholesteric layers of the director field (heli-layers) and the regularly stacked TGB slab-layers. Just as the usual Grandjean-Cano steps are known to be edge dislocations of the heli-layers, the new defects were identified as edge dislocations of the slab-layers. Their core structure was qualitatively described in the case of strong anchoring conditions as a new kind of defect wall in which some of the TGB screw dislocation lines leave the grain boundaries to travel parallel to the smectic planes and form local edge dislocations.

More accurate experiments would allow us to determine the static elastic coefficients of the model. Two regimes have already been observed in the present experiments : at low thicknesses, the elastic energy of compression overtakes the wall energies and the ratio C (i.e. coupling over elasticity of the slab-layers) can be estimated. At higher thickness, the core energies dominate and the defects disappear. The limit allows us to estimate the defect energy relative to the twist energy.

These observations open new questions about the structure of the defects in TGB mesophases. More theoretical work is clearly needed to describe the core of the slab-dislocations completely, the localisation and the energy of the core are unknown.

Anyway, whatever the core structure of the new defects, their observation within adjacent Grandjean-Cano lines provides a new optical characterization of all the TGB phases in thin wedges.

Acknowledgments.

The present work has benefitted from helpful discussions with M. Brunet, Y. Galerne, P. Martinot-Lagarde and J. Prost and received financial support from the Groupe de Recherche CNRS « Cristaux liquides et polymères cristaux liquides ferroélectriques ».

References

[1] de Gennes P. G., *Solid State Commun.* **10** (1972) 753.
[2] Renn S. R. and Lubensky T. C., *Phys. Rev.* **A 38** (1988) 2132.
[3] Renn S. R. and Lubensky T. C., *Mol. Cryst. Liq. Cryst.* **209** (1991) 349.
[4] Renn S. R., *Phys. Rev.* **A 45** (1992) 953.
[5] Goodby J. W., Waugh M. A., Stein S. M., Chin E., Pindak R. and Patel J. S., *Nature* (London) **337** (1989) 449 ; *J. Am. Chem. Soc.* **111** (1989) 8119.
[6] Slaney A. T. and Goodby J. W., *J. Mat. Chem.* **1** (1991) 5.
[7] Slaney A. T. and Goodby J. W., *Liq. Cryst.* **9** (1991) 849.
[8] Nguyen H. T., Twieg R. J., Nabor M. F., Isaert N. and Destrade C., *Ferroelectrics* **121** (1991) 187.
[9] Bouchta A., Nguyen H. T., Achard M. F., Hardouin F., Destrade C., Twieg R. J., Maaroufi A. and Isaert N., *Liq. Cryst.* **12** (1992) 57S.

[10] Nguyen H. T., Bouchta A., Navailles L., Barois P., Isaert N., Twieg R. J., Maaroufi A. and Destrade C., *J. Phys. II France* **2** (1992) 1889.
[11] Ihn K. J., Zasadzinski A. N., Pindak R., Slaney A. J. and Goodby J. W., *Science* **258** (1992) 275.
[12] Navailles L., Barois P. and Nguyen H. T., *Phys. Rev. Lett.* **71** (1993) 545 ; *ibid.* **72** (1994) 1300.
[13] Brunet M. and Isaert N., *Ferroelectrics* **84** (1988) 25.
[14] Grandjean F., *C.R. Acad. Sci., Paris* **172** (1921) 71.
[15] Cano R., *Bull. Soc. Fr. Minér. Cristallogr.* **90** (1967) 333.
[16] Orsay Liquid Crystal Group, *Phys. Lett.* **A 28** (1969) 687.
[17] de Gennes P. G., The Physics of Liquid Crystals (Clarendon Press, Oxford, 1974).
[18] Meyer R. B., Stebler B. and Lagerwall S. T., *Phys. Rev. Lett.* **41** (1978) 1393.
[19] Nallet F. and Prost J., *Europhys. Lett.* **4** (1987) 307.
[20] Richetti P., Kékicheff P., Parker J. L. and Ninham B. W., *Nature* **346** (1990) 252.
[21] de Gennes P. G., *C.R. Acad. Sci., Paris B* **275** (1972) 939.
[22] Pershan P. S., *J. Appl. Phys.* **45** (1974) 1590.
[23] Kléman M., Points Lignes Parois (Les Editions de Physique, Les Ulis 1977).